www.sciencemag.org/cgi/content/full/science.1221054/DC1

Supplementary Materials for

The Heliosphere's Interstellar Interaction: No Bow Shock

D. J. McComas,* D. Alexashov, M. Bzowski, H. Fahr, J. Heerikhuisen, V. Izmodenov, M. A. Lee, E. Möbius, N. Pogorelov, N. A. Schwadron, G. P. Zank

*To whom correspondence should be addressed. E-mail: dmccomas@swri.edu

Published 10 May 2012 on *Science* Express
DOI: 10.1126/science.1221054

This PDF file includes:

Supplementary Text
Supporting online material – S1

Geometric Relationship of Interstellar Neutral Flow Vector Angles

In the plane of the trajectories, the angle θ_∞ (true anomaly at infinity), swept out by the interstellar bulk flow trajectory from infinity to its perihelion at 1 AU, is related to the observer location and the ISM flow direction as follows:

$$\theta_\infty = \lambda_{\mathrm{ISM}\infty} + 180^o - \lambda_{\mathrm{Peak}} \qquad \text{(S1-1)}$$

Because the inflow angle in latitude $\beta_{\mathrm{ISM}\infty}$ is rather small (-4.98±0.21^o), λ_{Peak}, the location of the ISM bulk flow peak is taken in ecliptic longitude with negligible effect on the results. For the hyperbolic trajectory of the incoming interstellar bulk flow in the Sun's gravitational field, the angle θ_∞ swept out by the radius vector of the trajectory from infinity to perihelion at 1 AU is related to the bulk speed at infinity $V_{\mathrm{ISM}\infty}$ by

$$\frac{-1}{\cos\theta_\infty} = 1 + \frac{R_E V_{ISM\infty}^2}{GM_S} = 1 + \frac{V_{ISM\infty}^2}{V_E^2} \quad or: \; V_{ISM\infty} = \sqrt{\frac{GM_S}{R_E}\left(\frac{-1}{\cos\theta_\infty} - 1\right)} \; = \; V_E\sqrt{\frac{-1}{\cos\theta_\infty} - 1}$$

or: (S1-2)

$$\theta_\infty = \cos^{-1}\left(-1/\left(1 + \frac{R_E V_{ISM\infty}^2}{GM_S}\right)\right) = \cos^{-1}\left(-1/\left(1 + \frac{V_{ISM\infty}^2}{V_E^2}\right)\right)$$

where R_{E} is the distance from the Sun to the Earth and M_{s} the Sun's mass. Equation (S1-2) establishes a fixed relation between $V_{\mathrm{ISM}\infty}$ and θ_∞ (and by inference through (S1-1) between $V_{\mathrm{ISM}\infty}$ and $\lambda_{\mathrm{ISM}\infty}$) that hinges solely on celestial mechanics. A smaller angle θ_∞ (or $\lambda_{\mathrm{ISM}\infty}$) is equivalent to a higher speed $V_{\mathrm{ISM}\infty}$ at infinity and vice versa. Combining (S1-1) and (S1-2) we get: (S1-3)

$$\lambda_{ISM\infty} = \lambda_{Peak} - 180^o + \cos^{-1}\left(-1/\left(1 + \frac{R_E V_{ISM\infty}^2}{GM_S}\right)\right) = \lambda_{Peak} - 180^o + \cos^{-1}\left(-1/\left(1 + \frac{V_{ISM\infty}^2}{V_E^2}\right)\right)$$

Equation (S1-3) prescribes a relation between $\lambda_{ISM\infty}$ and $V_{ISM\infty}$ that is based solely on celestial mechanics and contains only one free parameter, i.e. λ_{Peak}.

Similarly, we can also formulate an analytical relationship that connects the observed peak latitude, Ψ_{Peak}, of the bulk flow with the ISM inflow latitude, $\beta_{ISM\infty}$, at infinity via the angle θ_∞. As shown in (15), the ISM flow direction in latitude in the rest frame at 1 AU Ψ_{Peak} is geometrically related to the inflow direction in latitude at infinity $\beta_{ISM\infty}$ through:

$$\tan\psi_{Peak} = \frac{\tan\beta_{ISM\infty}}{|\sin\theta_\infty|} \tag{S1-4}$$

As for equation S1-1, this equation, used in (15) and (16), applies exactly only for angles along the trajectory taken in the ecliptic. Again, because $\beta_{ISM\infty}$ is so small, any difference in angles over the entire bounding range are $<0.1^o$. The peak directions in the rest frame and in the observer frame are related as follows:

$$\frac{\sin\psi'_{Peak}}{V_{ISM}(1AU)} = \frac{\sin(\psi_{Peak} - \psi'_{Peak})}{V_E} \tag{S1-5}$$

Because $V_{ISM}(1AU)$ depends on $V_{ISM\infty}$ and thus is related to $\lambda_{ISM\infty}$ via (S1-1) and (S1-2), an observation of ψ'_{Peak} at the ISM flow maximum location yields a relation $\beta_{ISM\infty}(\lambda_{ISM\infty})$. Equation (S1-4) appears to suggest a simple linear relationship between $\tan(\beta_{ISM\infty})$ and $\sin(\lambda_{ISM\infty} + 180^o - \lambda_{Peak})$ with only one free parameter Ψ_{Peak}, where λ_{Peak} is already known from (S1-3).

The observable is indeed ψ'_{Peak}, which is connected with Ψ_{Peak} through equation (S1-5) and thus the ISM flow speed at infinity, $V_{ISM\infty}$, and ultimately $\lambda_{ISM\infty}$. However, the transformation from the rest frame into the moving frame produces only a minute

variation of Ψ_{Peak} as a function of $\lambda_{\mathrm{ISM}\infty}$. Yet, because we are evaluating equations (S1-4) and (S1-5) for a value of θ_∞ that is far from 0, a small offset ($\tan\beta_0$) in $\tan\beta_{\mathrm{ISM}\infty}$ is required when using equation (S1-4) as a linear approximation in the variables shown, i.e. equation (S1-4) is modified to read:

$$\tan\beta_{ISM\infty} = \tan\beta_0 + \tan\psi_{Peak}\cdot|\sin(\lambda_{ISM\infty} + 180^o - \lambda_{Peak})| \qquad \text{(S1-6)}$$

Now, we can use equation (S1-6) for a fit to $\beta_{\mathrm{ISM}\infty}(\lambda_{\mathrm{ISM}\infty})$ values, as obtained with either the analytical or the test particle method. As a result, we have two fit parameters that we can compare, and we can use a simplified relation for the best values.

Resulting Relations for the Interstellar Neutral Flow Parameters

Equation (S1-3) is determined by celestial mechanics and contains only one free parameter, i.e. λ_{Peak}. With the analytical method this parameter was determined directly from the observations as the location of the maximum ISM flux in ecliptic longitude as $\lambda_{\mathrm{Peak}} = 130.6^{\mathrm{o}}$ averaged over 2009 and 2010 (16). With the test particle method a group of best fitting parameter sets was found in a combined χ^2 minimization that follows closely the same relation, as can be seen in Figures 22 and 23 of (17), but they don't describe exactly the analytical relation. Therefore, we have fitted equation (S1-3) to the results of (17), with λ_{Peak} as a free parameter, with a resulting value $\lambda_{\mathrm{Peak}} = 129.8^{\mathrm{o}}$. However, the test particle simulations have been carried out by tracing the neutral atom trajectories from 1 AU to 150 AU, while the analytical calculations were carried out from 1 AU to infinity. While the latter is an idealized treatment, neutral atoms from the interstellar medium travel to 1 AU largely collisionless from distances larger than 1000 AU. Therefore, small but noticeable differences in the derived arrival direction and original

speed of the particles arise in the two different methods, and we have extrapolated the remaining trajectories from 150 AU to infinity with an analytical calculation. This leads to small adjustments in the inflow longitude $\lambda_{ISM\infty}$ and the inflow speed $V_{ISM\infty}$ for the test particle results, thus modifying the ISM flow peak location from (17) to $\lambda_{Peak} = 130.21^o$. Using the analytical method, we had to obtain the peak location by extrapolating the neutral fluxes to the location in each orbit where the IBEX spin axis points exactly at the Sun in the ecliptic plane, whereas the best fitting values were obtained from a test particle method using all available data simultaneously. This necessarily leads to a larger uncertainty for λ_{Peak} in the analytical determination. With full error propagation, an uncertainty of $\Delta\lambda = 0.7^o$ is given by (16), while the χ^2 minimization leads to $\Delta\lambda = 0.35^o$ in (17). In the following, we have derived a weighted mean between the two complementary determinations and a combined uncertainty that again considers the individual uncertainties by their weighting and the deviation of the individual results as an additional quadratic contribution to the uncertainty. This combination of results leads to: $\lambda_{Peak} = 130.29 \pm 0.47^o$, which can be inserted into equation (S1-3) to establish the current best $V_{ISM\infty}(\lambda_{ISM\infty})$ relation

(S1-7)

$$\lambda_{ISM\infty} = -49.71 \pm 0.47^o + \cos^{-1}(-1/(1+\frac{R_E V_{ISM\infty}^2}{GM_S})) = -49.71 \pm 0.47^o + \cos^{-1}(-1/(1+\frac{V_{ISM\infty}^2}{V_E^2}))$$

To arrive at this equation, we have combined 180^o and $\lambda_{Peak} = 130.29 \pm 0.47^o$. In the comparison with data, both methods used the actual distance of the Earth from the Sun and orbital speed, while the average values are used for parameterization in the equations. Figure S1 shows $V_{ISM\infty}$ as a function of $\lambda_{ISM\infty}$ for the mean value along with the curve as derived by the analytical method and the best values obtained from the test particle

method. The combined uncertainties are shown for the mean curve. As can be seen, the two methods provide a very close match in their results. The combined uncertainty overlaps with both determinations.

The combination of equations (S1-4) and (S1-5) provides a similar unique analytical relation between $\lambda_{ISM\infty}$ and $\beta_{ISM\infty}$. However, the relation is more complex and can only be solved implicitly. Therefore, we have approximated this relation with equation (S1-6), which contains two free parameters for a linear least square fit, i.e. $\tan\beta_o$ and $\tan\psi_{Peak}$. In this case, we have fitted both the analytical results by (16) and the test particle results by (17) separately, and then obtained weighted mean values in a similar way as above for λ_{Peak}. Because the uncertainty of the peak location in latitude is largely determined by observational uncertainties, both methods carry approximately the same uncertainty. It should be noted that tracing to only 150 AU in the test particle method leads to a negligible deviation in this parameter, and no correction is necessary. We find as a mean: $\tan\beta_o$ = -0.030, $\tan\psi_{Peak}$ =-0.073, and an uncertainty $\Delta\beta_{ISM\infty} = 0.21^o$, thus resulting in:

$$\tan\beta_{ISM\infty} = -0.030 - 0.073 \cdot |\sin(\lambda_{ISM\infty} + 180^o - \lambda_{Peak})| \qquad \text{(S1-8)}$$

Figure S2 shows $\beta_{ISM\infty}$ as a function of $\lambda_{ISM\infty}$ in a similar representation as Fig. S1. Again, the different results agree with the mean and each other within the combined uncertainty around the mean curve.

As shown in (16), the temperature T_∞ is also tied to the inflow longitude $\lambda_{ISM\infty}$ in a similar way as the inflow speed and latitude are. To arrive at a simplified functional description for the temperature, we make use of the fact that the temperature can be expressed in terms of the Mach number M_∞ of the flow, which itself only depends weakly on the inflow longitude $\lambda_{ISM\infty}$, as can be seen in Fig. 8 of (16).

$$T(\lambda_{ISM\infty}) = \frac{V^2_{ISM\infty}(\lambda_{ISM\infty}) \cdot m_{He}}{M^2_{\infty}(\lambda_{ISM\infty}) \cdot \gamma \cdot k} \quad \text{(S1-9)}$$

γ is the adiabatic index, k is the Boltzmann constant, and m_{He} the mass of He. Here we have again computed mean values between the temperature determinations in (16) and (17), where we have used the temperatures with a minimum correction for the data transfer limitations between IBEX-Lo and the central electronics unit of IBEX (as described in the Appendix B of (16)). Further analysis of the interface and the data system has shown that such a minimum correction appears to be close to actual behavior. To account for remaining uncertainties, we have quadratically added the typical difference between the two independent temperature determinations to the statistical uncertainty. We have then computed the square of the Mach number as a function of $\lambda_{ISM\infty}$, which we fitted linearly according to:

$$M^2_{\infty}(\lambda_{ISM\infty}) = a_0 + a_1 \cdot \lambda_{ISM\infty} \quad \text{(S1-10)}$$

We found $a_0 = -13.5$ and $a_1 = 0.489$ as the best fitting values, thus leading to

$$T(\lambda_{ISM\infty}) = \frac{290.5 \cdot V^2_{ISM\infty}(\lambda_{ISM\infty})}{(a_0 + a_1 \cdot \lambda_{SM\infty})} = \frac{290.5 \pm 19 \cdot V^2_{ISM\infty}(\lambda_{ISM\infty})}{(-13.5 + 0.489 \cdot \lambda_{SM\infty})} \quad \text{(S1-11)}$$

where $V_{ISM\infty}(\lambda_{ISM\infty})$ is taken from equation (S1-7). The uncertainties are combined in the coefficient 290.5 ± 19 in equation (S1-11). The temperature relation is shown in Fig. S3 in a similar representation as used in Figures S1 and S2. The uncertainties shown in equations S1-7, S1-8, and S1-11 and also used in Table 1 can be considered the 1σ uncertainties based on both complementary analyses (16, 17).

Both (16) and (17) derived an optimum value of $\lambda_{ISM\infty}$ = 79+3-3.5^o, based on χ^2 minimization, largely influenced by the dependence of the observed flow peak in ecliptic latitude as a function of observer longitude. The bounding range of -3.5º and +3.0º from this value was established in the χ^2 analysis based on conservative heuristic arguments as described in (16) and (17). This range cannot be directly expressed in terms of σ-uncertainties, but because of the conservative approaches taken it is likely equivalent to significantly larger than 1σ. (15) also demonstrated that the ratio of the angular widths of the flow distribution in longitude and latitude constrains $V_{ISM\infty}$, based on which (16) found a constraint consistent with the same angular range in $\lambda_{ISM\infty}$. Table 1 in the main paper compiles the most probable value of the flow vector and temperature along with the two bounding sets of values in ecliptic J2000 and galactic coordinates.

Supporting online material - S2

Derivation of the Shock Compression Ratio and Other Parameters at the Heliospheric Shock/Bow Wave

A plasma particle interacts with shock electromagnetic fields on the lengthscale of a few gyroradii r_g and on the timescale of a few gyroperiods τ_g. Therefore, an inhomogeneous non-stationary shock is locally planar and stationary if $r_g / R << 1$ and $\tau_g / T << 1$, where R and T are the spatial and temporal scales for variation of the shock front. These inequalities are valid at the heliospheric bow shock. Thus, we may consider the Rankine-Hugoniot (R-H) relations for an oblique planar stationary shock with shock normal in the x-direction. Since there is no net charge increase or decrease at the shock and $\nabla \times \mathbf{E} = 0$, $\mathbf{E}$ is conserved across the shock. Thus the upstream and downstream vectors **B** and **v** must lie in the same plane, the so-called coplanarity plane. Finally the observer may transform locally into the de Hofmann-Teller frame such that **B** and **v** are parallel both upstream and downstream of the shock. Without loss of generality we take $B_y = 0$ and $v_y = 0$. The R-H relations yield a cubic equation for the compression ratio X:

$$\left(M_{A1}^2 - X\cos^2\theta\right)^2 \left\{2\beta_1 X + M_{A1}^2\left[X(\gamma-1)-(\gamma+1)\right]\right\}$$

$$+M_{A1}^2 X\sin^2\theta\left\{X\cos^2\theta\left[X(\gamma-1)-(\gamma+1)\right]+M_{A1}^2\left[\gamma+X(2-\gamma)\right]\right\}=0, \qquad \text{(S2-1)}$$

where subscript 1 refers to upstream quantities and

$$\gamma = 5/3 \tag{S2-2}$$

$$M_{A1}^2 = v_{x1}^2 / v_{A1}^2 \tag{S2-3}$$

$$v_{A1}^2 = B_1^2 / 4\pi\rho_1 \tag{S2-4}$$

$$\cos^2\theta = B_{x1}^2 / B_1^2 \tag{S2-5}$$

$$\beta_1 = c_1^2 / v_{A1}^2 \tag{S2-6}$$

where c_1 is the upstream sound speed. If we set $X = 1$ in equation (S2-1), we obtain the phase velocities of the three MHD modes

$$v_{x1}^2 = v_{A1}^2 \cos^2\theta \tag{S2-7}$$

$$v_{x1}^2 = (1/2)\left\{v_{A1}^2 + c_1^2 \pm \left[(v_{A1}^2 + c_1^2)^2 - 4v_{A1}^2 c_1^2 \cos^2\theta\right]^{1/2}\right\} \tag{S2-8}$$

The ratio B_{z2} / B_{z1} characterizing the three shocks corresponding to the three MHD waves is given by

$$\frac{B_{z2}}{B_{z1}} = \left(Xv_{x1}^2 - \frac{B_{x1}^2 X}{4\pi\rho_1}\right)\left(v_{x1}^2 - \frac{B_{x1}^2 X}{4\pi\rho_1}\right)^{-1} \tag{S2-9}$$

Both numerator and denominator of equation (S2-9) are greater (less) than zero for the fast (slow) shock. For the numerator positive and the denominator negative we have the

intermediate wave. Thus it is clear that $B_{z2}/B_{z1} > 1$ for the fast shock and $B_{z2}/B_{z1} < 1$ for the slow shock. The fast shock satisfies

$$v_{x1}^2 > \frac{B_{x1}^2 X}{4\pi\rho_1}, \tag{S2-10}$$

whereas the slow shock satisfies

$$v_{x1}^2 < \frac{B_{x1}^2}{4\pi\rho_1}. \tag{S2-11}$$

In between these values is the domain of the intermediate wave. Thus it is easy to check whether the compression ratio we obtain numerically corresponds to the fast shock.

To construct our map of the bow shock/wave we specify c_1 and v_{A1} in the interstellar medium. As we discussed, a reasonable model for the shape of the bow wave near its nose is a sphere, presumably centered downstream of the Sun to account for the greater downwind extent of the termination shock. The polar (z) axis is oriented from the center of the sphere to the bow shock/wave nose. Using spherical coordinates the outward shock normal is

$$\mathbf{n} = \mathbf{i}\sin\vartheta\cos\phi + \mathbf{j}\sin\vartheta\sin\phi + \mathbf{k}\cos\vartheta, \tag{S2-12}$$

where ϑ is used to distinguish it from the angle θ between the shock normal and the magnetic field. In this coordinate system we orient the **i**-axis so that the interstellar magnetic field is

$$\mathbf{B}_1 = B_1(\mathbf{i}\sin\vartheta_0 + \mathbf{k}\cos\vartheta_0). \tag{S2-13}$$

Therefore, we have

$$\cos\theta = (\mathbf{B}_1 \cdot \mathbf{n})/B_1 = \sin\vartheta_0 \sin\vartheta\cos\phi + \cos\vartheta_0\cos\vartheta. \tag{S2-14}$$

Now we may evaluate the following parameters:

$$v_{x1}^2 = v_{ISM}^2 \cos^2\vartheta, \tag{S2-15}$$

$$M_{A1}^2 = (v_{ISM}^2 / v_{A1}^2)\cos^2\vartheta, \tag{S2-16}$$

where v_{ISM} is the speed of the interstellar plasma flow, which is normal to the bow shock at the nose. This may not be quite correct since the orientation of the magnetic field could shift the bow shock nose into a direction that is not quite parallel to the interstellar plasma flow. However, this subtlety is beyond the scope of this calculation.

Now the procedure is to choose a pair of values for the two angles (ϑ,ϕ). Using these values evaluate equations (S2-2) through ((S2-6) using equations (S2-14) through (S2-16). Insert these values into equation (S2-1) and evaluate X numerically. Check that the obtained value of X satisfies equation (S2-10). This should be continued for more values of (ϑ,ϕ) until a contour map of X values is continued out to a bounding contour where $X = 1$. Since, at this boundary, equation (S2-8) with the upper sign is satisfied, we may write

$$v_{ISM}^2 \cos^2\vartheta = (1/2)\left\{v_{A1}^2 + c_1^2 + \left[(v_{A1}^2 + c_1^2)^2 - 4v_{A1}^2 c_1^2 \left(\sin\vartheta_0 \sin\vartheta\cos\phi + \cos\vartheta_0 \cos\vartheta\right)^2\right]^{1/2}\right\}. \quad \text{(S2-17)}$$

This relation may be simplified to

$$\cos^4\vartheta - \frac{(v_{A1}^2 + c_1^2)}{v_{ISM}^2}\cos^2\vartheta + \frac{v_{A1}^2 c_1^2}{v_{ISM}^4}\left(\sin\vartheta_0 \sin\vartheta\cos\phi + \cos\vartheta_0 \cos\vartheta\right)^2 = 0 \quad . \quad \text{(S2-18)}$$

Equation (S2-17) or (S2-18) gives an analytical expression for the boundary beyond which the shock becomes a wave. It should coincide with the $X = 1$ contour line. Figure S4 shows the maximum compression ratio at the bow shock as a function of the interstellar magnetic field strength, which shows that the bow shock ceases to exist for field strengths less than 2.2 μG.

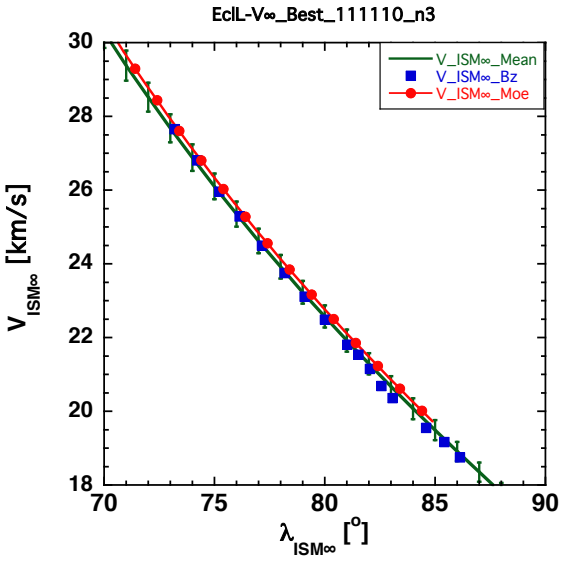

***Fig. S1**: $V_{ISM\infty}$ as a function of $\lambda_{ISM\infty}$ for the mean curve (green) with combined uncertainties, the analytical curve (red), and the optimum parameter sets obtained in the test particle method (blue).*

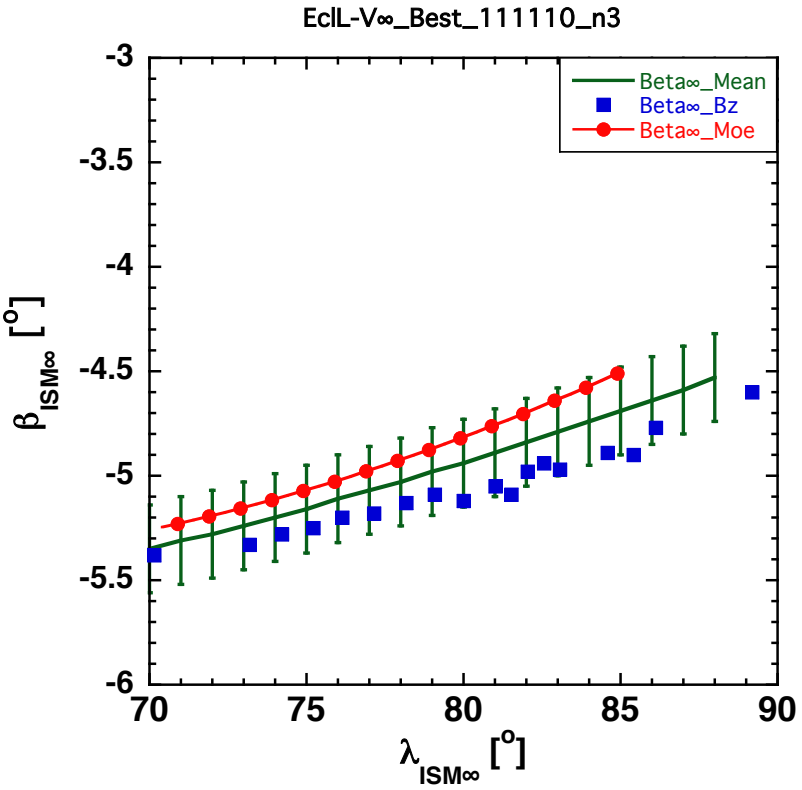

***Fig. S2**: $\beta_{ISM\infty}$ as a function of $\lambda_{ISM\infty}$ in a similar representation as Fig. S1*

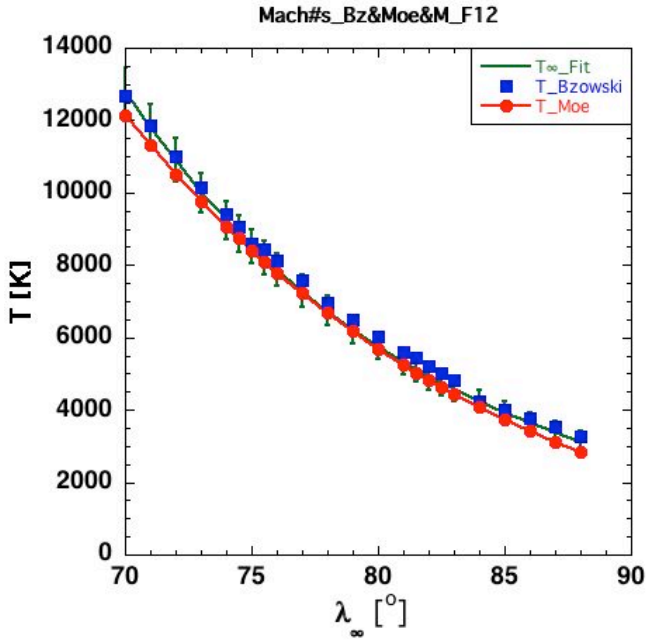

Fig. S3*: Interstellar temperature as a function of ecliptic longitude of the interstellar flow in a similar representation as Fig. S1 and S2.*

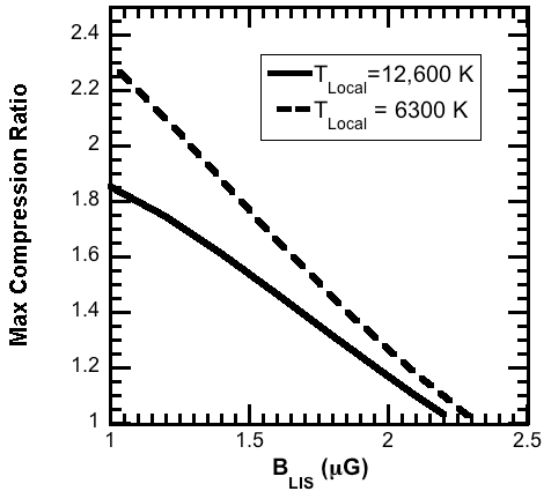

Fig. S4: *Maximum compression ratio (up- to downstream speed at bow shock) as a function of the local interstellar magnetic field strength for local interstellar temperatures of 6300 K (dashed curve) and 12,600 K (solid curve). The 6300 K temperature is that of the undisturbed local interstellar medium, while the higher 12,600 K temperature represents conditions near the bow shock where neutral atoms stream out from the heliosphere and become ionized, thereby heating the local interstellar plasma. We used a LISM proton density of 0.07 cm^{-3} and* ***v-B*** *angle of 48° and find that no bow shock exists for field strengths that exceed 2.2 μG.*

References and Notes

1. E. N. Parker, The stellar-wind regions. *Astrophys. J.* **134**, 20 (1961). doi:10.1086/147124

2. V. B. Baranov *et al*., *Sov. Phys. Dokl.* **15**, 791 (1971).

3. H. Fahr, Is the heliospheric interface submagnetosonic? Consequences for the LISM presence in the heliosphere. *Adv. Space Res.* **6**, 13 (1986). doi:10.1016/0273-1177(86)90378-9

4. H. Fahr, H. Fichtner, K. Scherer, Theoretical aspects of energetic neutral atoms as messengers from distant plasma sites with emphasis on the heliosphere. *Rev. Geophys.* **45**, RG4003 (2007). doi:10.1029/2006RG000214

5. V. V. Izmodenov *et al*., Kinetic-gasdynamic modeling of theheliospheric interface. *Space Sci. Rev.* **146**, 329 (2009). doi:10.1007/s11214-009-9528-3

6. M. A. Lee *et al*., Physical processes in the outer heliosphere. *Space Sci. Rev.* **146**, 275 (2009). doi:10.1007/s11214-009-9522-9

7. G. P. Zank *et al*., Physics of the solar wind–local interstellar medium interaction: Role of magnetic fields. *Space Sci. Rev.* **146**, 295 (2009). doi:10.1007/s11214-009-9497-6

8. D. J. McComas *et al*., IBEX—Interstellar Boundary Explorer. *Space Sci. Rev.* **146**, 11 (2009). doi:10.1007/s11214-009-9499-4

9. D. J. McComas *et al*., Global observations of the interstellar interaction from the Interstellar Boundary Explorer (IBEX). *Science* **326**, 959 (2009). doi:10.1126/science.1180906 Medline

10. N. A. Schwadron *et al*., Comparison of Interstellar Boundary Explorer observations with 3D global heliospheric models. *Science* **326**, 966 (2009). doi:10.1126/science.1180986 Medline

11. D. J. McComas *et al*., IBEX observations of heliospheric energetic neutral atoms: Current understanding and future directions. *Geophys. Res. Lett.* **38**, L18101 (2011). doi:10.1029/2011GL048763

12. S. A. Fuselier *et al*., The IBEX-Lo sensor. *Space Sci. Rev.* **146**, 117 (2009). doi:10.1007/s11214-009-9495-8

13. E. Möbius *et al*., Direct observations of interstellar H, He, and O by the Interstellar Boundary Explorer. *Science* **326**, 969 (2009). doi:10.1126/science.1180971 Medline

14. M. Hłond *et al*., Precision pointing of IBEX-Lo observations. *Astrophys. J.* **198**, 9 (2012). doi:10.1088/0067-0049/198/2/9

15. M. A. Lee *et al*., An analytical model of interstellar gas in the heliosphere tailored to Interstellar Boundary Explorer observations. *Astrophys. J.* **198**, 10 (2012). doi:10.1088/0067-0049/198/2/10

16. E. Möbius *et al*., Interstellar gas flow parameters derived from Interstellar Boundary Explorer-Lo observations in 2009 and 2010: Analytical analysis. *Astrophys. J.* **198**, 11 (2012). doi:10.1088/0067-0049/198/2/11

17. M. Bzowski *et al*., Neutral interstellar helium parameters based on IBEX-Lo observations and test particle calculations. *Astrophys. J.* **198**, 12 (2012). doi:10.1088/0067-0049/198/2/12

18. L. Saul *et al*., Local interstellar neutral hydrogen sampled in situ by IBEX. *Astrophys. J.* **198**, 14 (2012). doi:10.1088/0067-0049/198/2/14

19. P. Bochsler *et al*., Estimation of the neon/oxygen abundance ratio at the heliospheric termination shock and in the local interstellar medium from IBEX observations. *Astrophys. J.* **198**, 13 (2012). doi:10.1088/0067-0049/198/2/13

20. M. Witte, Kinetic parameters of interstellar neutral helium. *Astron. Astrophys.* **426**, 835 (2004). doi:10.1051/0004-6361:20035956

21. S. Redfield, J. Linsky, The structure of the local interstellar medium. IV. Dynamics, morphology, physical properties, and implications of cloud-cloud interactions. *Astrophys. J.* **673**, 283 (2008). doi:10.1086/524002

22. E. C. Stone *et al*., An asymmetric solar wind termination shock. *Nature* **454**, 71 (2008). doi:10.1038/nature07022 Medline

23. M. Opher, E. C. Stone, P. C. Liewer, The effects of a local interstellar magnetic field on Voyager 1 and 2 observations. *Astrophys. J.* **640**, L71 (2006). doi:10.1086/503251

24. H. Washimi, G. P. Zank, Q. Hu, T. Tanaka, K. Munakata, A forecast of the heliospheric termination-shock position by three-dimensional MHD simulations. *Astrophys. J.* **670**, L139 (2007). doi:10.1086/524358

25. R. Ratkiewicz, J. Grygorczuk, Orientation of the local interstellar magnetic field inferred from Voyagers' positions. *Geophys. Res. Lett.* **35**, L23105 (2008). doi:10.1029/2008GL036117

26. N. A. Schwadron *et al*., Separation of the Interstellar Boundary Explorer ribbon from globally distributed energetic neutral atom flux. *Astrophys. J.* **731**, 1 (2011). doi:10.1088/0004-637X/731/1/56

27. N. V. Pogorelov, J. Heerikhuisen, G. P. Zank, Probing heliospheric asymmetries with an MHD-kinetic model. *Astrophys. J.* **675**, L41 (2008). doi:10.1086/529547

28. J. Heerikhuisen, N. V. Pogorelov, V. Florinski, G. P. Zank, J. A. le Roux, The effects of a κ-distribution in the heliosheath on the global heliosphere and ENA flux at 1 AU. *Astrophys. J.* **682**, 679 (2008). doi:10.1086/588248

29. G. P. Zank, H. L. Pauls, L. L. Williams, D. T. Hall, Interaction of the solar wind with the local interstellar medium: A multifluid approach. *J. Geophys. Res.* **101**, 21639 (1996). doi:10.1029/96JA02127

30. K. G. Gayley, G. P. Zank, H. L. Pauls, P. C. Frisch, D. E. Welty, One- versus two-shock heliosphere: Constraining models with goddard high resolution spectrograph Lyα spectra toward α Centauri. *Astrophys. J.* **487**, 259 (1997). doi:10.1086/304600

31. V. Izmodenov, D. Alexashov, A. Myasnikov, Direction of the interstellar H atom inflow in the heliosphere: Role of the interstellar magnetic field. *Astron. Astrophys.* **437**, L35 (2005). doi:10.1051/0004-6361:200500132

32. R. Lallement *et al*., The interstellar H flow: Updated analysis of SOHO/SWAN data. *AIP Conf. Proc.* **1216**, 555 (2010). doi:10.1063/1.3395925

33. P. Frisch *et al*., The galactic environment of the Sun: Interstellar material inside and outside of the heliosphere. *Space Sci. Rev.* **146**, 235 (2009). doi:10.1007/s11214-009-9502-0

34. D. J. McComas, N. A. Schwadron, An explanation of the Voyager paradox: Particle acceleration at a blunt termination shock. *Geophys. Res. Lett.* **33**, L04102 (2006). doi:10.1029/2005GL025437